On the emergence of critical regions at the onset of thermoacoustic instability in a turbulent combustor

Vishnu R. Unni, Abin Krishnan, R. Manikandan, Nitin B. George, R. I. Sujith, Norbert Marwan, and Jürgen Kurths

Vishnu R. Unni, Abin Krishnan, R. Manikandan, Nitin B. George, R. I. Sujith, Norbert Marwan, and Jürgen Kurths

On the emergence of critical regions at the onset of thermoacoustic instability in a turbulent combustor

Vishnu R. Unni,[1,a)] Abin Krishnan,[1] R. Manikandan,[1] Nitin B. George,[1] R. I. Sujith,[1] Norbert Marwan,[2] and Jürgen Kurths[2,b)]

[1]*Indian Institute of Technology Madras, Chennai 600036, India*
[2]*Potsdam Institute for Climate Impact Research, Potsdam 14412, Germany*

We use complex network theory to investigate the dynamical transition from stable operation to thermoacoustic instability via intermittency in a turbulent combustor with a bluff body stabilized flame. A spatial network is constructed, representing each of these three dynamical regimes of combustor operation, based on the correlation between time series of local velocity obtained from particle image velocimetry. Network centrality measures enable us to identify critical regions of the flow field during combustion noise, intermittency, and thermoacoustic instability. We find that during combustion noise, the bluff body wake turns out to be the critical region that determines the dynamics of the combustor. As the turbulent combustor transitions to thermoacoustic instability, during intermittency, the wake of the bluff body loses its significance in determining the flow dynamics and the region on top of the bluff body emerges as the most critical region in determining the flow dynamics during thermoacoustic instability. The knowledge about this critical region of the reactive flow field can help us devise optimal control strategies to evade thermoacoustic instability. *Published by AIP Publishing.* https://doi.org/10.1063/1.5028159

Emergence of order from chaos is a common sight in nature. Synchronous flashing of fireflies, Mexican wave in a football stadium, triggering of riots, collective behaviour of a school of fish or a swarm of birds, emergence of consciousness from the interplay of millions of neurons, and the evolution of life are some of the examples seen in nature. Formation of convection cells, pattern formation in the Belousov–Zhabotinsky reaction, and the emergence of coherent vortices in a turbulent flow are examples of order emerging from disorder in fluid systems.[1–3] An important fluid dynamic system exhibiting the emergence of order from disorder is a combustor, which houses a confined turbulent reactive flow. During normal operation, the reactive flow field exhibits incoherent turbulent fluctuations. However, under certain operational conditions, the flow field reorganizes, and a spatially ordered periodic behavior emerges. During this dynamic regime known as thermoacoustic instability, the acoustic field inside the combustor exhibits dangerous large amplitude oscillations. In this paper, using complex spatial networks, we characterize the spatial dynamics of the combustor during the stable operation (chaotic oscillations), the thermoacoustic instability (limit cycle oscillations), and the transition regime from stable operation to thermoacoustic instability known as intermittency. Further, using network measures, we identify the critical regions of the reactive flow field that influences the dynamics of the reactive flow field during thermoacoustic instability.

I. INTRODUCTION

The interaction between unsteady combustion and the acoustic field in the combustor is inevitable in engineering systems such as boilers, gas turbine engines, and rocket engines. Such an interaction manifests as high amplitude self-excited oscillations when the energy added from the unsteady combustion to the acoustic field of the confinement overcomes the acoustic losses in the system.[4] This phenomenon is known as thermoacoustic instability or combustion instability. We encounter thermoacoustic instability in solid rocket motors,[5] liquid rocket motors,[6] ramjets,[7] afterburners,[8] and power generating gas turbine engines.[9] Thermoacoustic instability engenders violent vibrations which damage the sensors, increase thermal stresses to combustor walls, induce fatigue failure of components, trigger flame blow-off, and flashback leading to a costly shutdown or catastrophic damage of components and probably mission failures.[9]

The coupling amongst acoustics, hydrodynamics, and flame dynamics during thermoacoustic instability leads to complex spatiotemporal dynamics. The complex behavior of a thermoacoustic system, involving different length and time scales, arises due to different factors such as molecular mixing, turbulence, chemical kinetics, acoustic, and flame-flow interactions. Analysis of the spatiotemporal dynamics during thermoacoustic instability is vital in understanding the mechanism leading to thermoacoustic instability and devising passive control strategies for its mitigation.

Many of the early studies have focussed on the emergence of coherent structures at the onset of thermoacoustic instability. Various studies suggested that during thermoacoustic instability, vortices that shed periodically from the flame holders (bluff body, dump plane, etc.) induce periodicity in the heat release rate.[7,10,11] Smith and Zukoski[12] and

---

a)Electronic mail: vishnu.runni@gmail.com
b)Also at Department of Physics, Humboldt University Berlin, Newtonstr. 15, 12489 Berlin, Germany and Institute for Complex Systems and Mathematical Biology, University of Aberdeen, Aberdeen AB 24 UE, United Kingdom

Poinsot *et al.*[13] suggested that the large velocity fluctuations inside the combustor during thermoacoustic instability were the reason for the emergence of such vortices. Further, they identified that the process of formation and shedding of such vortices is closely correlated with the unsteadiness in pressure and heat release rate fluctuations. Smith and Zukoski,[12] through their study in a dump combustor, observed that during thermoacoustic instability, heat release rate fluctuations and pressure oscillations at the dump plane are in phase from the initiation of vortex formation, until the vortex has grown, propagated downstream, and impinged against the combustor wall. A review of thermoacoustic instability related to vortex shedding can be found in Schadow and Gutmark,[14] Coats,[15] and Renard *et al.*[16]

The transition from stable combustion to thermoacoustic instability exhibits interesting temporal dynamics.[17] Lieuwen[18] reported that depending upon operational parameters, a thermoacoustic system can exhibit both subcritical and supercritical Hopf bifurcations leading to thermoacoustic instability. This description of loss of stability of a fixed point at the onset of thermoacoustic instability is perfectly valid for laminar systems. However, for a turbulent combustor, Nair *et al.*[19] suggested that the low amplitude aperiodic oscillations characterizing stable combustion is deterministic chaos and Tony *et al.*,[20] through surrogate analysis, showed that this indeed is the case. This indicates that in turbulent combustors, the stable operation of a combustor (also called combustion noise) may not correspond to a fixed point and hence the onset of thermoacoustic instability cannot be considered as a Hopf bifurcation.

Nair *et al.*[21] showed that a turbulent combustor undergoes transition from stable combustion to thermoacoustic instability via intermittency. During combustion noise, the acoustic pressure is characterised by low amplitude aperiodic oscillations. Whereas, during thermoacoustic instability, the acoustic pressure signal is characterized by high amplitude periodic oscillations representing order. Intermittency is a state represented by bursts of high amplitude periodic oscillations embedded amidst regions of low amplitude aperiodic oscillations, albeit in a random manner. Using recurrence quantification analysis, Nair and Sujith[22] identified homoclinic orbits in the reconstructed phase space during intermittency. Nair and Sujith[23] also showed that combustion noise displays scale invariance and has multifractal signature that disappears at the onset of thermoacoustic instability. Gotoda *et al.* used tools from nonlinear time series analysis such as surrogate data analysis, permutation entropy, multifractal analysis, and translation error to characterise the onset of thermoacoustic instability.[24–26]

All the above studies on the transition to thermoacoustic instability have been performed on time series of state variables of the system. Some studies have concentrated on spatiotemporal dynamics during the transition to thermoacoustic instability. Taamallah *et al.*[27] studied the mean flame configuration during different dynamical regimes of a swirl stabilized combustor. The authors noted that the mean flame configuration changes at the onset of thermoacoustic instability. Hong *et al.*[28] investigated the recirculation zone structure and the flame stability during the transition to

thermoacoustic instability. During stable combustion, the recirculation zone consists of a primary and a secondary eddy. At the onset of thermoacoustic instability, the secondary eddy almost collapses and the flame starts to exhibit periodic flapping motion. The study highlighted the importance of the size and structure of the recirculation zone on flame stability. Recently, Unni and Sujith[29] studied the flame dynamics during intermittency prior to and post thermoacoustic instability. Even though the dynamical nature of intermittency (type II) was the same prior to both thermoacoustic instability and lean blowout, the flame dynamics exhibited significant differences. Mondal *et al.*[30] performed a spatiotemporal analysis of a turbulent combustor during the transition from combustion noise to thermoacoustic instability via intermittency. By calculating the instantaneous phase difference between the acoustic pressure and the local heat release rate oscillations, they observed that the aperiodic oscillations during combustion noise are phase asynchronous, while the high amplitude periodic oscillations characterizing thermoacoustic instability are phase synchronous. During intermittency, the coexistence of regions of desynchronized aperiodic oscillations and synchronized periodic oscillations resembling a chimera state is observed.

Most of the aforementioned studies focused on the flow and flame dynamics during thermoacoustic instability. These studies emphasized the formation of large coherent structures during thermoacoustic instability. However, there has been no study, till date, which brought to light the relative importance of different regions in a turbulent reactive flow field in determining the spatiotemporal dynamics of the turbulent combustor during the intermittency route to thermoacoustic instability. The aim of the present study is to identify critical regions in the flow field of a turbulent combustor during the transition from stable combustion (combustion noise) to unstable combustion (thermoacoustic instability) via intermittency using tools from complex network theory.

This study is based on the premise that a turbulent combustor can be considered as a complex system. In a turbulent combustor, the local interaction between the parts of the reactive flow results in the onset of self-organized, periodic oscillations known as thermoacoustic instability. This corresponds to an emergence of ordered and periodic spatiotemporal behaviour during thermoacoustic instability from a disordered and aperiodic state during combustion noise. Systems that exhibit such collective behaviour resulting from self-organization of the parts of the system which interact with each other are known as complex systems. Complex network theory has emerged as one of the popular tools to study complex systems. Barabasi, one of the pioneers in the field of network science, in his commentary in Nature Physics[31] stated: "Therefore, if we are ever to have a theory of complexity, it will sit on the shoulders of network theory." In network theory, the components of a complex system are represented as nodes and their interactions are represented as links between the nodes. Complex network theory, born in the twilight of the twentieth century with the discovery of small world networks[32] and scale free networks,[33] has found applications across disciplines such as computer

science, biology, medicine, economics, engineering, climate studies, and sociology.[34–38]

The previous decade has witnessed the application of complex network theory for temporal analysis of turbulent flows. Gao and Jin[39] used community detection algorithm to identify flow patterns in a two phase flow. Charakopoulos *et al.*[40] distinguished the various dynamical regimes of a heated turbulent jet using network properties. The scale-free nature of the combustion noise generated from a turbulent reactive flow was investigated by Murugesan and Sujith[41] using complex networks. They showed that the transition from combustion noise to thermoacoustic instability is reflected in the topology of the visibility network constructed from pressure time series as a transition from scale-free to order and used the network measures to get precursors to an impending thermoacoustic istability.[42] The high dimensional nature of thermoacoustic instability has been brought to light by Okuno *et al.*[43] using cycle networks and phase space networks. Godavarthi *et al.*[44] and Gotoda *et al.*[45] used recurrence networks to study the topology of the phase space corresponding to different dynamical states of a turbulent combustor.

Recently, complex networks have been used to study the spatiotemporal dynamics of fluid systems, in particular, climate systems. Scientists used measures such as Pearson correlation, mutual information, and event synchronization between time series to quantify the degree of statistical interdependence of different spatial regions.[46] Tsonis and Roebber[37] constructed a correlation based climate network from the global temperature field. The authors observed that the overall dynamics of the global climate system is the result of the interaction between two interweaved subnetworks: one operating in the tropics and the other at higher altitudes with the equatorial network acting as the agent connecting the two hemispheres. Malik *et al.*[38] used a nonlinear synchronization measure, known as event synchronization,[47] to construct a spatial network for the spatiotemporal analysis of extreme monsoonal rainfall over Indian subcontinent. The network properties used in this study helped to visualize the structure of the extreme event rainfall fields, identification of water vapor pathways, and moisture sinks. In addition, the methodology of spatial network construction using event synchronization has been used to establish a prediction scheme for extreme floods in the eastern central Andes.[48]

Molkenthin *et al.*[49] performed spatial network analysis of prototypical flows and an ocean flow in the tropical Pacific region. In the case of prototypical flows, the authors solved the advection diffusion equation and used the resulting temperature field to calculate the statistical interdependence between any two nodes in the flow field. The authors used a continuous analytical analogue of Pearson correlation to compute the correlation matrix. In the case of real flows, they computed the correlation matrix from the sea surface temperature using standard correlation. The analysis unravelled a relationship between the underlying velocity field and complex network measures. High values of degree coincided with high velocity field and high values of betweenness centrality marked the transition zones between regions of different magnitudes or directions of the underlying velocity field.

The above study, however, was restricted only to stationary flows. Tupikina *et al.*[50] extended this analysis to a varying flow model with a time dependent velocity field. Taira *et al.*[51] used the concept of the Biot Savart law to construct a spatial network based on vortical interactions in a two dimensional decaying isotropic turbulent field obtained from direct numerical simulations. The resulting vortical interaction network is characterized by a weighted scale-free network. Scarsoglio and Iacobello[52] constructed a correlation network from kinetic energy time series on a three dimensional forced isotropic turbulent field obtained from direct numerical simulation. The authors identified coherent patterns in the flow field using network properties.

These promising studies have motivated us to perform spatial network analysis on a turbulent reactive flow field during the intermittency route to thermoacoustic instability. To that end, we performed experiments in a backward facing step combustor with a bluff body as the flame holding device. Simultaneous acoustic pressure measurements, high speed flame imaging, and particle image velocimetry (PIV) are performed during combustion noise, intermittency, and thermoacoustic instability, respectively. A spatial network is then constructed based on the correlation between the velocity time series at each of the three dynamical regimes of combustor operation. We closely follow Molkenthin *et al.*[49] and Tupikina *et al.*[50] in the procedure for network construction. Complex network measures are then computed to identify critical regions in the flow field.

The rest of the paper is organized as follows: the experimental setup and the measurement techniques employed in the present study is detailed in Sec. II. The methodology of network construction is elaborated in Sec. III. Section IV presents the results and discussion which is followed by concluding remarks in Sec. V.

II. EXPERIMENTAL SETUP AND PROCEDURES

Our experiments were performed in a backward facing step, bluff body stabilized combustor. The experimental rig consists of a settling chamber, a burner of 40 mm diameter, and a combustion chamber of cross section 90 mm × 90 mm and length 1100 mm. The experimental setup is the same as the one used in the study of Unni and Sujith.[29] The schematic of the experimental setup is shown in Fig. 1.

The air enters the test section through the settling chamber, which is provided to reduce the fluctuations in the inlet air. The fuel used in the experiments is liquefied petroleum gas (LPG, 40% Propane and 60% Butane), introduced into the combustion chamber through four radial holes of 1.7 mm diameter using a central shaft. A circular disk (bluff body) of 40 mm diameter and 10 mm thickness is used for flame stabilization. The partially premixed air–fuel mixture is spark ignited in the recirculation zone at the dump plane using an 11 kV ignition transformer. Mass flow controllers are used to measure and control the supply of fuel and air into the combustion chamber (Alicat Scientific, MCR Series, 100 SLPM model for fuel flow, 2000 SLPM for air flow; uncertainty is ±(0.8% of reading + 0.2% of full scale). In the current study, the fuel flow rate ($\dot{m}_f$) is fixed and the air flow rate
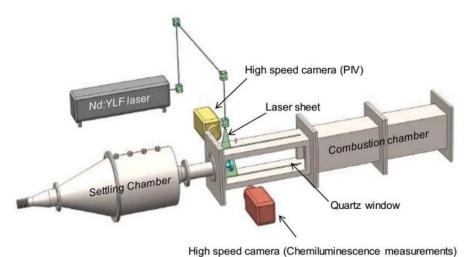
FIG. 1. The schematic of the backward facing step combustor used for the present study. A quartz window is used to facilitate high speed flame imaging and PIV. The design of the combustor was adapted from Ref. 53.

($\dot{m}_a$) is gradually increased, decreasing the equivalence ratio ($\varphi = (\dot{m}_f/\dot{m}_a)_{actual} / (\dot{m}_f/\dot{m}_a)_{stochiometry}$). The flow conditions are maintained such that the reactive flow is turbulent [$(1.09 \pm 0.01) \times 10^5 < Re < (2.12 \pm 0.01) \times 10^5$]. The unsteady pressure (P') is measured using a piezoelectric transducer (PCB 103B02, with sensitivity of 223.4 mV/kPa and an uncertainty of ± 0.15 Pa), located at a distance of 20 mm downstream of the dump plane at a sampling frequency of 10 kHz for 3 s. To facilitate optical diagnostics, a pair of quartz windows (400 mm × 90 mm × 10 mm) is provided in the side walls of the combustion chamber. The optical diagnostic techniques applied in the present study include high speed imaging of flame chemiluminescence [field of $\dot{q}'(x, y)$] and particle image velocimetry (PIV). Both these techniques are elaborated in the Appendix.

III. CONSTRUCTION OF THE SPATIAL NETWORK

In the present study, the turbulent reactive flow field is divided into a regular grid. Each grid point is considered as a node of a complex network. Two nodes are connected when the correlation between the time series of velocity corresponding to each node is above a particular threshold. The velocity field is obtained from PIV as described in the Appendix.

In this study, we consider two types of correlations to construct two different types of network. In the first approach, we use the Pearson correlation coefficient defined as

$$R_p = \frac{\sum_{i=1}^{n}(x_i - \bar{x})(y_i - \bar{y})}{\sqrt{\sum_{i=1}^{n}(x_i - \bar{x})^2}\sqrt{\sum_{i=1}^{n}(y_i - \bar{y})^2}}, \qquad (1)$$

where x_i is the element of one velocity time series at a grid point and y_i is the element of another velocity time series at a different grid point. The index i represents the time stamp. The arithmetic means of both time series are represented by $\bar{x}$ and $\bar{y}$, respectively. Two nodes of the network are connected if the Pearson correlation coefficient between the corresponding time series of velocity is above a threshold (R_{pt}). We chose R_{pt} by analysing the link density of the network

for different values of R_{pt}. The link density (ρ) of a network refers to the ratio of actual number of links to the maximum possible number of links. If N is the number of nodes of a network and E is the actual number of links in the network, the link density is given by

$$\rho = \frac{2E}{N(N-1)}, \qquad (2)$$

where $N(N-1)/2$ is the maximum number of possible links of the given undirected network. In the current analysis, R_{pt} is chosen as 0.25, since at this value, the variation in link density is maximum between combustion noise, intermittency, and thermoacoustic instability. Maximum variation in link density ensures maximum variability in network topology as the turbulent combustor transitions from combustion noise to thermoacoustic instability via intermittency which, in turn, will be reflected in the spatial distribution of network properties.

In the second approach, the network is constructed based on the dot product defined as

$$R_s = \sum_{i=1}^{n} x_i y_i. \qquad (3)$$

In Pearson correlation, two time series are correlated when the fluctuations of both time series vary in a similar fashion, i.e., they could have very different amplitudes but still have high correlation. Whereas, in the case of dot product, two time series are correlated when the fluctuations vary in a similar fashion and have similar amplitudes. While R_p lies between -1 and 1, R_s can assume any real value depending upon the magnitude of variables. Hence, unlike in the case of network construction using R_p, where we choose R_{pt} as 0.25, for the approach using dot product, we fix the link density of the network, (R_{st}), at 50%. This implies that 50% of total possible links are present in the network corresponding to the different dynamical regimes of combustor operation. Like the fixed correlation coefficient approach, the fixed link density approach also ensures that the topology of the network changes as the turbulent combustor undergoes transition from one dynamical regime to another and helps us to

compare and contrast the spatiotemporal dynamics across the three regimes of combustor operation. Both of these approaches of constructing spatial networks help to discern different aspects of the flow field. This is further elaborated in Sec. IV.

An adjacency matrix, A, represents a spatial network constructed as described above. Its elements A_{ij} ($i, j = 1, 2, \ldots, N$) are equal to one when a link l_{ij} exists between the ith and j^{th} node and zero otherwise. A thus obtained is a symmetric matrix since the correlation network is undirected (i.e., i connected to j implies j connected to i).

In order to compare the topology of different networks, we use some basic measures to characterize the spatial networks. The degree (k_i) of a node (grid point) i gives the number of grid points linked to a particular grid point

$$k_i = \sum_{j=1}^{N} A_{ij}. \tag{4}$$

A grid point having higher degree than others is expected to have a stronger influence on the functioning of the network. The interconnectivity of the neighbours of a grid point i is quantified by the local clustering coefficient

$$C_i = \frac{2E_i}{k_i(k_i - 1)}, \tag{5}$$

where E_i is the number of links between the neighbours of the grid point i and $k_i(k_i - 1)/2$ is the maximum number of links possible among the neighbours. It gives an estimate of the spatial continuity of the correlations in the velocity field.

Like degree, another measure that highlights the importance of a grid point i is betweenness centrality (b_i). It is the sum of the ratios of the number of shortest paths between any two grid points passing through a particular grid point to the total number of shortest paths between those two grid points

$$b_i = \sum_{j,k \in N, j \neq k} \frac{n_{jk}(i)}{n_{jk}}, \tag{6}$$

where $n_{jk}(i)$ is the number of shortest paths between j and k passing through the grid point i. Physically, b_i of a node indicates the extend of information passed through that node, if we assume that the information travels through the shortest paths in the network. An additional node centrality measure is closeness centrality (c_i) which measures the inverse of the mean shortest path length from a node to all other nodes. If the shortest path between a grid point i to all other grid points j connected to it is $d(i, j)$, then closeness centrality is given by

$$c_i = \sum_{j \in N, j \neq i} 2^{-d(i,j)}. \tag{7}$$

Physically, closeness centrality measures speed of information propagation in the network. For example, if any disturbance is given to a grid point with the highest c_i, the disturbance will travel to other grid points in a minimum amount of time. In the present study, we have used the Python package called *pyunicorn* to compute all the aforementioned network properties.[46]

IV. RESULT AND DISCUSSIONS

The present study explores the use of spatial network analysis on a turbulent reactive flow field. We perform the spatial network analysis, based on two different approaches, i.e., the Pearson correlation and the dot product. We analyze three different dynamical regimes of a turbulent combustor, stable combustion (combustion noise), intermittency, and thermoacoustic instability. At each of these dynamical states, we investigate the spatial distribution of four network parameters, degree, local clustering coefficient, betweenness centrality, and closeness centrality across the turbulent reactive flow field. Before going into the investigation of network properties, we describe the turbulent reactive flow field during the dynamical regimes of combustion noise, intermittency, and thermoacoustic instability with the help of particle image velocimetry.

A. The dynamics of the turbulent reactive flow

During combustion noise, the fuel flow rate and air flow rate are maintained at 30 SLPM and 480 SLPM, respectively ($\varphi = 0.98$). The low amplitude aperiodic pressure fluctuations characterizing combustion noise is depicted in Fig. 2 along with some instantaneous snapshots of the vorticity field (curl of velocity) superimposed on the velocity field corresponding to the points (a)–(e) marked on the pressure signal. The flow exiting the burner section enters the combustion chamber and gets deflected due to the presence of the bluff body. It further recirculates in the wake of both the bluff body and the dump plane. However, the magnitude of velocity in the wake of the bluff body is higher when compared to that in the wake of the dump plane. From the tip of the bluff body, small vortices are shed in a random manner during combustion noise.

During intermittency, the air flow rate is increased to 570 SLPM, keeping the fuel flow rate constant ($\varphi = 0.82$). The flow dynamics during the aperiodic [Figs. 3(a)–3(c)] and periodic regime [Figs. 3(d)–3(i)] during intermittency is illustrated in Fig. 3. Compared to combustion noise, two major differences are observed in the flow dynamics during intermittency, specifically, during the periodic regime. First, coherent structures are formed in the wake of the dump plane during periodic epochs of intermittency, which are absent during the aperiodic epochs. Second, the vortices shed from the tip of the bluff body are larger when compared to the ones shed during combustion noise and aperiodic regime of intermittency.

During thermoacoustic instability, we maintain the air flow rate at 750 SLPM and the fuel flow rate at 30 SLPM ($\varphi = 0.63$). High amplitude periodic pressure fluctuations, with a frequency of 143 Hz, along with the instantaneous snapshots of the flow field corresponding to one cycle of the periodic oscillation are shown in Fig. 4. We notice the periodic formation of large coherent structures in the wake of the dump plane similar to what is reported in earlier studies.[14] These coherent structures propagate downstream, impinge on the bluff body and the combustor wall, enhancing fine
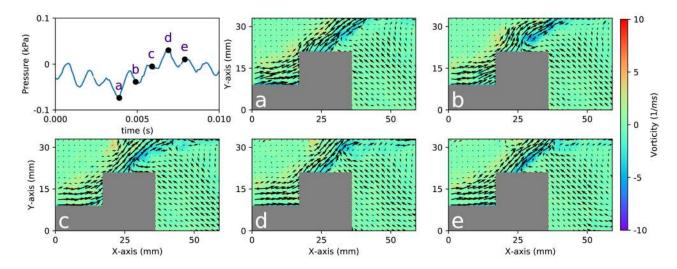
FIG. 2. Instantaneous snapshots of the vorticity field superimposed on the velocity field corresponding to the points (a)–(e) marked on the time series of fluctuating pressure during combustion noise.

scale mixing of unburned gas and hot radicals leading to periodic bursts of high heat release rate.

The acoustic power produced locally can be indicated by the distribution of the acoustic power production index (R_{xy}) of the reactive flow field defined as

$$R_{xy} = \int_0^t P' \dot{q}'(x, y) dt, \tag{8}$$

where P' is the acoustic pressure fluctuation and $\dot{q}'(x, y)$ is the unsteady heat release rate at the point (x, y). The average
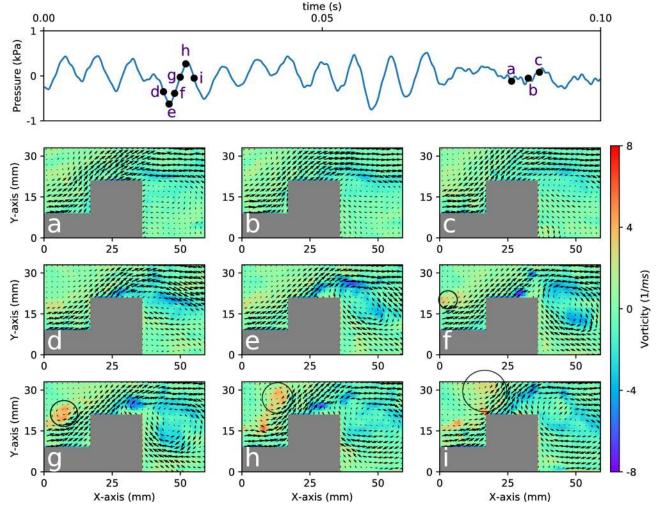

FIG. 3. Instantaneous snapshots of the vorticity field superimposed on the velocity field corresponding to the regime of intermittency. During the aperiodic epochs of intermittency, no large coherent structure is observed [(a)–(c)]. However, during the periodic part of intermittency, we observe large coherent vortices in the flow field [(f)–(i)]. The black circles mark the vortices shed from the dump plane traveling downstream towards the bluff body.
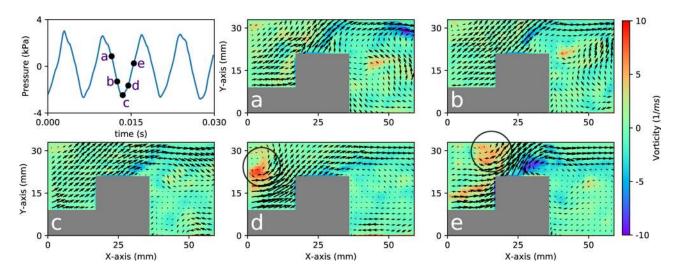
FIG. 4. Instantaneous snapshots of the vorticity field superimposed on the velocity field corresponding to the points (**a**)–(**e**) marked on the time series of fluctuating pressure during thermoacoustic instability.

vorticity field superimposed on the average velocity field and R_{xy} during combustion noise, intermittency, and thermoacoustic instability are shown in Fig. 5. During combustion noise, in the average flow field, we observe that there are two shear layers present in the flow field marked by highly positive (red) and highly negative (blue) vorticity. We refer to the shear layer marked by red color as the outer shear layer and the shear layer marked by blue color as the inner shear layer. These shear layers divide the flow into three regions, namely, region A-the wake of the dump plane, region B-the region between the outer shear layer and the inner shear layer, called as "shear zone," and region C-the bluff body wake, as shown in Fig. 5(a). Note that the locations of high acoustic power production during thermoacoustic instability coincide with the locations having high values of average vorticity. In this paper, we further explore this link by analyzing the reactive flow field at the different dynamic regimes using spatial networks.

B. Spatial network analysis

In the present study, as explained in III, we have considered two methods of network construction: (a) using Pearson correlation and (b) using dot product. The manner in which the spatial network is constructed determines the meaning that we can associate with network properties.

In a turbulent reactive flow field, the correlations in velocity between two points in the flow field will die down beyond a critical distance between them. However, during thermoacoustic instability, there is an emergence of large-scale coherent structures which can induce correlations between parts of the flow that are far apart. Such correlations are captured using the Pearson correlation. Consider two points in the flow field that are far apart and have very different amplitudes for velocity fluctuations. If the velocities at these locations vary in a similar manner, then these two locations are connected in the network constructed using Pearson correlation. Such long-range connections are only possible
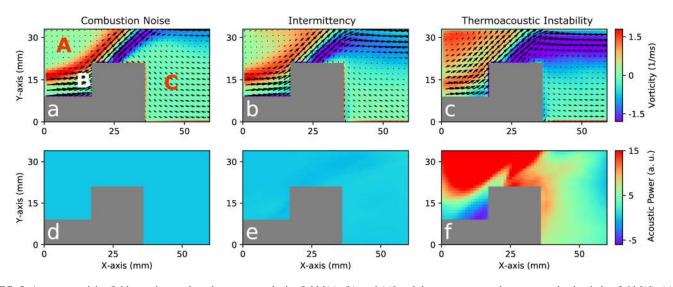

FIG. 5. Average vorticity field superimposed on the average velocity field [(a), (b), and (c)] and the average acoustic power production index field [(d), (e), and (f)] during combustion noise, intermittency, and thermoacoustic instability. During thermoacoustic instability, regions of high average acoustic power production coincide with regions of high average vorticity present in the wake of the dump plane upstream of the bluff body.

when the turbulent flow embodies large-scale coherent structures. Thus, the connectivity patterns of a network constructed using Pearson correlation capture both the presence and absence of large scale coherent structures in the flow field and the local correlations. However, when we consider dot product, only the velocity fluctuations of comparable amplitudes are correlated. This can happen mostly for points that are nearby in the flow field. In this manner, we capture both short and long range connections in the network constructed based on Pearson correlation and only the local connections in networks constructed based on dot products. Network measures obtained for both of these spatial networks thus provide different informations about the flow topology.

1. Topology of spatial networks constructed using Pearson correlation

The degree of a node gives the number of neighbors of that particular node in the spatial network. In the case of the spatial network constructed using Pearson correlation, very high degree implies that the correlation between the velocity fluctuations at the given grid point (here, a grid point in the flow field is the node) and that of a large number of other grid points is above the threshold correlation (R_{p_t}). The

spatial distribution of degree during the three dynamical regimes of the turbulent combustor is shown in Figs. 6(a)–6(c). During combustion noise, region C is having the highest degree but both regions A and B are having very low degree. During combustion noise, the flow recirculates in the wake of the bluff body (Fig. 2). This coherent motion of the fluid particles in the wake of the bluff body during combustion noise gives the region a very high degree distribution [Fig. 6(a)]. During intermittency, the degree of the shear zone increases [Fig. 6(b)]. During thermoacoustic instability, the shear zone has the highest degree, whereas the degree of the bluff body wake reduces [Fig. 6(c)]. The dump plane wake has a medium degree with a region of very low degree located at the top left corner. As the turbulent combustor transitions from combustion noise to thermoacoustic instability, the degree of the bluff body wake reduces and that of the shear zone (region B) and dump plane wake (region A) increase.

Next, the spatial distribution of *local clustering coefficient* (C_i) during the three dynamical regimes of the turbulent combustor operation is shown in Figs. 6(d)–6(f). C_i of a grid point gives the idea of connectivity among the neighbors of that grid point. High values of C_i for a grid point imply that the neighbors of the grid point are highly interconnected.
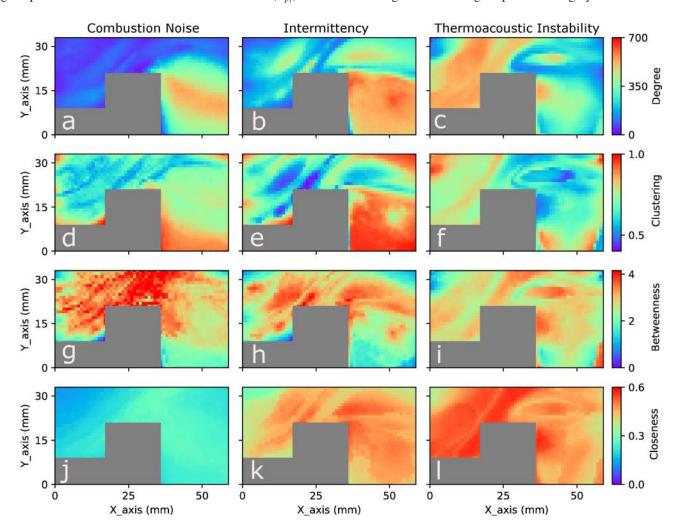

FIG. 6. Spatial distribution of degree, local clustering coefficient, betweenness and closeness during combustion noise, intermittency, and thermoacoustic instability obtained by constructing a spatial network using Pearson correlation keeping the threshold correlation coefficient at 0.25.

From a flow perspective, this implies that the correlation between the velocity fluctuations of the neighbors of a given grid point is above a threshold. If a region is having high degree and high C_i, then, we can say that the given region is spatially coherent in terms of velocity fluctuations. During combustion noise, the region C has some patches of high C_i. Both regions A and B have low and medium values of C_i [Fig. 6(d)]. During intermittency, the most of the bluff body wake has very high C_i [Fig. 6(e)]. High values of degree and C_i for the bluff body wake, during intermittency, imply that the grid points of the region are having large number of neighbors that are highly interconnected to each other. During thermoacoustic instability [Fig. 6(f)], the shear zone along with some regions of the bluff body wake has the lowest C_i. Very high value of C_i along with very low degree for the corner of dump plane wake, during thermoacoustic instability, suggests that even though this region of very low average velocity and very high average vorticity has very few neighbors, these neighbors are highly interconnected to each other. Very high value of degree and medium value of C_i for the shear zone, during thermoacoustic instability, suggests that the nodes in the shear zone have a large number of neighbors which are moderately interconnected among themselves.

Betweenness centrality (b_i) of a grid point gives the fraction of all the shortest paths for every pair of grid points in the flow field passing through the given grid point. High values of b_i highlight the main pathways of information travel in a network if it is assumed that information propagates through shortest paths in a network. In the present analysis, the regions of high b_i indicate those locations that connect different parts of the flow that are otherwise uncorrelated to each other. Considering this, regions of high b_i could be responsible for the increased correlation in the reactive flow field during an ordered behavior like thermoacoustic instability.

During combustion noise, in the case of the spatial network constructed using Pearson correlation, the region of high b_i is spread across the reaction field [Fig. 6(g)]. During intermittency, b_i is high along the shear zone (region B) and in the part of flow neighbouring to the shear zone [Fig. 6(h)]. During thermoacoustic instability, the shear zone, along with some regions in the bluff body wake, shows a very high value of b_i [Fig. 6(i)]. High values of degree and b_i coupled with very low value of C_i for the shear zone, during thermoacoustic instability, imply that the grid points in the shear layer have a large number of neighbours, spread across the entire flow field, with very low interconnections among them. We can thus hypothesize that the shear zone acts as a bridge through which the flow fluctuations are transported, between the dump plane wake and the bluff body wake during thermoacoustic instability.

Closeness centrality c_i of a grid point measures the closeness of that particular grid point to all other grid points in the flow field. It is proportional to the reciprocal of the sum of shortest path lengths between a grid point and all other grid points in the flow field. Any perturbation given to a grid point with the highest value of c_i travels in minimum time to all other grid points of the flow field. We observe that during combustion noise, the bluff body wake (region

C) has higher closeness centrality [Fig. 6(j)] compared to the rest of the flow field. Thus, any perturbation given to any grid points in the bluff body wake will alter the dynamics of combustion noise. Due to the very high value of degree and c_i, we can infer that the bluff body wake is the most critical region during combustion noise. During intermittency, the c_i of the bluff body wake is similar to that of the shear zone (region B) [Fig. 6(k)]. During thermoacoustic instability, c_i of the bluff body wake is lower than that of the shear zone (region B) [Fig. 6(l)]. The c_i of the shear zone, as the turbulent combustor under goes transition from combustion noise to thermoacoustic instability, reaches the maximum value. The shear zone with very high values of degree, b_i and c_i, emerges as the most critical region during thermoacoustic instability. We can thus hypothesize that any control measure directed towards mitigation of thermoacoustic instability will be most effective when applied to the shear zone, i.e., region B.

2. Emergence of critical regions at the onset of thermoacoustic instability

In the past, many studies have investigated the flow pattern in the wake of a flame holder during combustion noise and thermoacoustic instability.[7,12,13] During stable combustion, the incoming reactant mixture separates from the surface of the flame holder and mixes with the hot products recirculating in the wake region downstream of the flame holder in a thin turbulent shear layer. This process is the key for maintaining continuous ignition and establishing a stable propagating flame. During thermoacoustic instability, the shear layer formed downstream of the flame holder is perturbed periodically by large coherent structures which dictate the dynamics of the reactive flow field. Hence, the recirculating wake downstream of the flame holder, which is critical for stabilizing the turbulent flame during the regime of stable operation (combustion noise), loses its significance in determining the dynamics of the reactive flow field during thermoacoustic instability.

The importance of the bluff body (flame holder) wake during combustion noise is very well captured by the spatial network analysis performed in the current study. It is reflected in the high values of degree and closeness centrality. The reflection of this finding in the distribution of centrality measures across the flow field corroborates our methodology of spatial network construction. As the turbulent combustor transitions to thermoacoustic instability, the bluff body wake (region C) loses its importance and the region between the outer and inner shear layer (region B) emerges as the most important region in the flow field. During intermittency, even though the bluff body wake (region A) still has high values of degree and closeness centrality, the values of these centrality measures increase for the shear zone (region B) when compared to that during combustion noise. Hence, the spatial network analysis is able to capture the transition of the turbulent combustor from combustion noise to thermoacoustic instability via intermittency effectively.

One important point to be noted here is regarding region A (the wake of the dump plane) not emerging as the most

critical region at the onset of thermoacoustic instability. It has to be emphasized here that the periodic formation of large coherent structures is seen in the wake of the dump plane during thermoacoustic instability. Also, the maximum value of Rayleigh index R_{xy}, an indicator of the local acoustic power production, also occurs in the wake of the dump plane (Fig. 5). However, region B emerges as the most critical region in determining the periodic dynamics of the reactive flow field during thermoacoustic instability.

The identification of the most critical regions at the onset of thermoacoustic instability is of paramount importance as this information can be used for devising efficient control strategies to mitigate thermoacoustic instability. Very recent studies have investigated the efficiency of control strategies based on the identification of critical regions obtained by using network centrality measures. Russo *et al.*[54] have applied spatial network analysis for the spatial distribution of fire breaks in heterogeneous forest landscapes for the control of wildland fires. The group of network nodes (small land patches) that favour fire propagation is identified by exploiting network centrality statistics such as betweenness centrality and Bonacich centrality. The authors, through simulations, have shown that the proposed methodology based on complex network approach outperforms the conventional forest management practices. Taira *et al.*[51] have shown that the two dimensional turbulence network, obtained by characterizing vortical interactions, is resilient against random perturbations but can be strongly influenced if the forcing is targeted towards large vortical structures which are identified as network hubs. This study highlights the advantage of using spatial network analysis for modifying the collective dynamics of vortices in the turbulent flow field as estimating and controlling each and every vortical structures in a turbulent flow are most likely improbable and impractical.

Analysis of networks constructed using Pearson's correlation suggests that for effectively mitigating thermoacoustic instability in the present turbulent combustor, the passive control strategies should be aimed at the region between the outer and inner shear layers which have high values of degree, betweenness centrality, and closeness centrality. This was identified by studying both long range and short range correlations in the flow field. In Sec. IV B 3, we will further analyze the flow field to identify the topology of connectivity introduced by local correlations in the flow field and compare and contrast those findings with the topology of networks constructed from Pearson's correlation.

3. Topology of the network constructed using dot product

In Secs. IV B 1 and IV B 2, we saw that the network constructed using Pearson correlation can identify the critical region of the flow field that determines the emerging large scale structure of the flow. One way to control such an emergent behaviour is to introduce passive perturbation into specific parts of the flow field such as micro jets and flow restrictors. Such perturbations spread locally in the flow field and affect the global behaviour of the flow field. Thus, it is important to study the local connectivity patterns of the flow field to identify such critical regions. To that end, we construct spatial networks using dot product as opposed to Pearson correlation. While Pearson correlation captures the connectivity patterns due to both local correlations and long range correlations induced by large scale flow structures, dot product captures mainly the local connectivity patterns.

The degree distribution during the different dynamical regimes of combustor operation is shown in Figs. 7(a)–7(c). During combustion noise, the degree distribution is very high along the region between the outer and inner shear layers (region B) which implies that the region is locally correlated to many other grid points in the flow field [Fig. 7(a)]. This implies that the amplitude of the velocities in the region between the outer and inner shear layer and its neighbors are correlated. Very high values of degree and medium values of local clustering coefficient between the outer and inner shear layer imply that the grid points in this region are connected to many other grid points in the flow field and these grid points are moderately interconnected to each other. During intermittency, the region between the outer and inner shear layer still continues to have high degree [Fig. 7(b)]. During thermoacoustic instability, the region between the outer and inner shear layer with very high degree expands to a larger area [Fig. 7(c)]. This suggests that a larger part of the flow field has velocity fluctuations of similar amplitude, possibly due to the periodic shedding of coherent structures during thermoacoustic instability.

A region with high degree and high clustering coefficient implies that the given region is spatially coherent in velocity amplitude. During combustion noise, the local clustering coefficient is very low for a small region in the wake of the dump plane (region A) and very high downstream of the bluff body (region C) [Fig. 7(d)]. The region between the outer and inner shear layer (region B) has medium values of clustering coefficient. During intermittency, the medium values of clustering coefficient extend towards the wake of the bluff body [Fig. 7(e)]. However, during thermoacoustic instability, the region between the outer and inner shear layer with medium values of local clustering coefficients shrinks [Fig. 7(f)]. This implies that as the turbulent combustor undergoes transition from combustion noise to thermoacoustic instability, the number of grid points in the region between outer and inner shear layer with moderately connected neighbours reduces.

During combustion noise, the betweenness centrality is very high in the region between the outer and inner shear layer (region B) [Fig. 7(g)]. This implies that a large number of shortest paths pass through the grid points in the region between the outer and inner shear layer. During intermittency also, the region between the outer and inner shear layer has the highest betweenness centrality [Fig. 7(h)]. However, during thermoacoustic instability, very high value of betweenness centrality shrinks to the part of region B on the top the bluff body [Fig. 7(i)].

In the case of the spatial network constructed using dot product, the closeness centrality is very low during both combustion noise and intermittency [Figs. 7(j) and 7(k)]. However, during thermoacoustic instability, the closeness
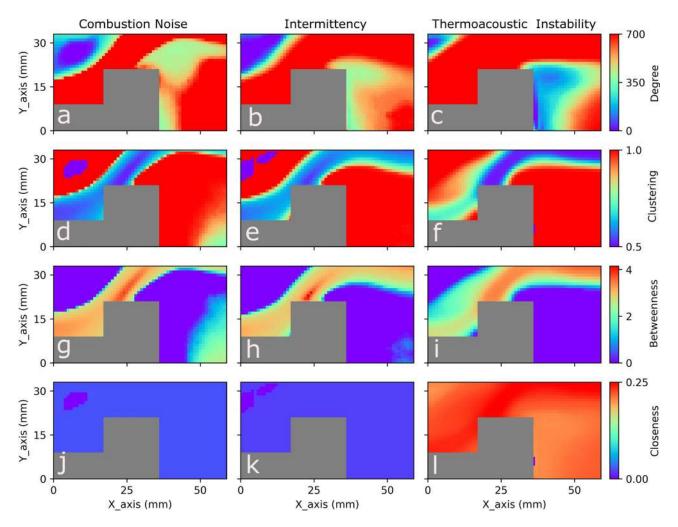
FIG. 7. Spatial distribution of degree, local clustering coefficient, betweenness and closeness during combustion noise, intermittency and thermoacoustic instability obtained by constructing a spatial network using dot product keeping the link density to be 50%.

centrality is very high [Fig. 7(l)]. Hence, as the turbulent combustor transits from combustion noise to thermoacoustic instability, the closeness centrality of the entire flow field increases. Thus, during thermoacoustic instability, if we give any perturbation to the flow field at any of the grid points, it affects the entire flow field in a very short period of time.

The findings from analysing the topology of network constructed using dot product suggest that during thermoacoustic instability, the significance of region B in determining the flow dynamics increases. Further, we observe that betweenness centrality is maximum in the part of region B lying on the top of the bluff body. This suggests that this part of the region B determines the dynamics during thermoacoustic instability both through local and long range correlations.

From the perspective of reactive flow, this location is where the vortices shed from the dump plane impinge and produce bursts of high heat release rate.[29] These bursts of high heat release rate translate into maximum acoustic power production in that location and also make this region the part of the flow that separates the region of high acoustic power production from the rest of the flow [Fig. 6(f)]. It is well known that the acoustic power production is enabled by the oscillatory behavior of the heat release rate. Since the region

on the top of the bluff body is where the burst of oscillations of heat release rate happen, it is interesting that this region also emerges as the most critical region in determining the dynamics of the reactive flow field.

V. CONCLUSION

In the present study, we have performed spatial network analysis on a bluff body stabilized turbulent combustor during the transition from stable combustion to thermoacoustic instability via intermittency. During each of these three dynamical regimes of combustor operation, a spatial network is constructed based on the correlation between the velocity time series obtained from particle image velocimetry (PIV) using both Pearson correlation and dot product. Complex network measures such as degree, local clustering coefficient, betweenness centrality, and closeness centrality are analysed during the transition from combustion noise to thermoacoustic instability.

We mainly find that during combustion noise, the network centrality measures such as degree and closeness centrality are very high for the bluff body wake suggesting that the dynamics during combustion noise is controlled by the bluff body wake. During intermittency, the bluff body

wake still retains its importance. Other regions of the flow field such as the dump plane wake and the region between the outer and inner shear layer have higher values of network centrality measures during intermittency when compared to that at combustion noise. However, during thermoacoustic instability, the bluff body wake loses its importance. Whereas the shear zone, the region between the outer and inner shear layer, which was the least important region during combustion noise with very low values of degree and closeness, emerges as the most critical region during thermoacoustic instability. The present analysis suggests that the region downstream of the dump plane which witnesses periodic formation of large coherent structures during thermoacoustic instability is not the most critical region in determining the flow dynamics during thermoacoustic instability. It is the region between the outer and inner shear layer that controls the dynamics during thermoacoustic instability. The analysis of topology of spatial network constructed based on dot product suggests that the part of the flow in the shear zone on top of the bluff body is possibly the ideal location for control strategies to be applied upon to mitigate thermoacoustic instability.

ACKNOWLEDGMENTS

APPENDIX: OPTICAL DIAGNOSTIC TECHNIQUES

A high speed CMOS camera (Phantom - v 12.1) is used to capture the OH* chemiluminescence with a narrow bandwidth filter centred at 308 nm (FWHM ±12). The images are acquired at a frame rate of 2000 Hz with a resolution of 800 × 600 pixels. The exposure time is chosen as 500 μs. The camera is outfitted with a 50 mm ZEISS camera lens at f/2 aperture. A measurement domain of 59 mm × 33 mm is captured on 743 × 416 pixels of the camera sensor. This region is located at 28 mm downstream of the dump plane. A total of 5000 images are captured at each of the three dynamical regimes of combustor operation, namely, combustion noise, intermittency, and thermoacoustic instability.

We obtain Mie scattering images for the high speed PIV. The flow is seeded with TiO_2 (Kronos make - product - 1071) particles of diameter 1 μm. We chose this size of the seeding particle such that it faithfully follows the fluid flow. However, the test section windows get clouded due to the small size of the particles. Hence, at each run of an experiment, we record the data only for one or two equivalence ratios depending on the clouding of the test section windows. The flow is illuminated with a single cavity double pulsed Nd:YLF (Neodymium-doped yttrium lithium fluoride) laser (Photonics) with a wavelength of 527 nm and a pulse duration

of 110 ns. The repetition rate of each of the two pulses is 2 kHz. The laser beam is directed towards the test section using a set of right angle prisms and a pair of convex lenses of focal length 500 mm and 50 mm. The laser beam is then expanded into a laser sheet of 2 mm thickness using 600 mm spherical lens and −16 mm cylindrical lens. The laser sheet enters the test section through a narrow slit (400 mm × 5 mm) made up of quartz, located on top of the combustion chamber. The time delay between the two pulses is carefully chosen between 15 and 25 μs for various equivalence ratios (or flow rates) such that the maximum pixel displacement of the particles between the two laser pulses is approximately in the range of 4–7 pixels. We ensure that the maximum displacement does not exceed $1/4^{th}$ of the size of the interrogation window. These parameters are chosen to avoid in plane loss of particles during the PIV evaluation. The Mie scattering image pairs are captured using a high-speed CMOS camera (Photron FASTCAM SA4), synchronized with the laser, outfitted with a ZEISS camera lens of 100 mm focal length with aperture at f/5.6. The camera can be operated at a maximum of 1024 × 1024 pixel resolution. The image pairs are captured at a frame rate of 1000 Hz. The measurement domain of length 59 mm and width 33 mm, located at the centre span of the bluff body, covers a region of 968 pixels × 541 pixels on the sensor. A bandpass optical filter centred at 527 nm (FWHM 10 nm) is placed in front of the camera to filter the flame and other background luminosity. The scattered light from the particles is roughly distributed over two pixels. A medium particle image density is ensured for all the flow rates.

The Mie scattering images were processed using PIV view software. The velocity vectors are calculated using a cross-correlation algorithm with a grid refining multi pass approach and least square Gauss fit peak search scheme.[55] For high equivalence ratios (low flow rates), we start the multipass analysis with 192 × 192 pixels grid size and ended with 32 × 32 pixels grid size. A 50% overlap is chosen between the interrogation windows. However, for lower equivalence ratios (higher flow rates), the analysis was started with 192 × 192 pixels followed by 4 passes and ended with a final grid size of 48 × 48 pixels to reduce the loss of correlation. An overlap of 65% is chosen between the interrogation windows for these flow rates. The pixel displacement, ideally, should be $1/4^{th}$ of the size of the interrogation windows used for PIV. However, we are restricted in reducing the size of the interrogation windows, to obtain the ideal pixel displacement of $1/4^{th}$ of the interrogation window, due to the medium density of particles in the field of view which could result in more outliers. We chose the grid size and the overlap such that the resolution of the velocity field is approximately the same for all the flow rates. This results in a vector spacing of approximately 1 mm for all the flow rates.

Post processing algorithms are used to detect and replace a small number of spurious vectors. First, to detect spurious vectors, we used the maximum displacement test with appropriate thresholds for different flow rates.[56] This is based on the expected bulk flow velocities in the test section. Additionally, a vector difference filter, which calculates the magnitude of the vector difference of a particular vector in

question to each of its eight neighbours, is also used to detect spurious vectors.[56] A threshold of two pixels is chosen for the vector difference filter. In total, less than 1% of the total velocity vectors are detected as spurious vectors and replaced with values obtained from bilinear interpolation. The uncertainty in the PIV evaluation arises out of the choice of the short pixel displacement. For the chosen methods of analysis of PIV images, estimation accuracies of the order of $1/10^{th}$ to $1/20^{th}$ pixels are realistic for 32×32 pixel samples from 8 bit digital images. The velocity uncertainty, in the current study, is approximately between 1.25% and 2.5% based on subpixel resolution between 0.05 and 0.1 for 32×32 interrogation windows[56] for low flow rates where the size of the interrogation window is 32×32 pixels. However, for higher flow rates, the uncertainty in velocity measurements could increase to 5% due to the use of 48×48 interrogation windows. For the current study, we present the data obtained from simultaneous pressure, high speed flame imaging, and PIV measurements at three different equivalence ratios corresponding to combustion noise ($\varphi = 0.98$), intermittency ($\varphi = 0.82$), and thermoacoustic instability ($\varphi = 0.63$), respectively.

[1] J. C. Mcwilliams, "The emergence of isolated coherent vortices in turbulent flow," J. Fluid Mech. **146**, 21–43 (1984).

[2] S. Strogatz and A. W. Edwards, "Sync-how order emerges from chaos in the universe, nature, and daily life," Math. Intell. **27**, 89–89 (2005).

[3] B. Hof and N. B. Budanur, "Searching for order in turbulent flow," Physics **10**, 25 (2017).

[4] R. Sujith, M. Juniper, and P. Schmid, "Non-normality and nonlinearity in thermoacoustic instabilities," Int. J. Spray Combust. Dyn. **8**, 119–146 (2016).

[5] F. Culick, "Combustion instabilities in solid propellant rocket motors," Tech. Rep. No. RTO-EN-023 (CALIFORNIA INST OF TECH PASADENA, 2004).

[6] F. E. Culick and V. Yang, "Overview of combustion instabilities in liquid-propellant rocket engines," Liq. Rocket Engine Combust. Instab. **169**, 3–37 (1995).

[7] D. E. Rogers and F. E. Marble, "A mechanism for high frequency oscillations in ramjet combustors and afterburners," Jet Propul. **26**, 456–462 (1956).

[8] A. M. Trout, W. K. Koffel, and G. R. Smolak, "Investigation of afterburner combustion screech and methods of its control at high combustor pressure levels," 1956.

[9] T. C. Lieuwen and V. Yang, *Combustion Instabilities in Gas Turbine Engines(Operational Experience, Fundamental Mechanisms and Modeling)*, Progress in Astronautics and Aeronautics (AIAA, 2005).

[10] W. Kaskan and A. Noreen, "High-frequency oscillations of a flame held by a bluff body," ASME Trans. **77**, 855–891 (1955).

[11] I. Elias, "Acoustical resonances produced by combustion of a fuel-air mixture in a rectangular duct," J. Acoust. Soc. Am. **31**, 296–304 (1959).

[12] D. A. Smith and E. E. Zukoski, "Combustion instability sustained by unsteady vortex combustion," AIAA Paper No. 85-1248, 1985.

[13] T. J. Poinsot, A. C. Trouve, D. P. Veynante, S. M. Candel, and E. J. Esposito, "Vortex-driven acoustically coupled combustion instabilities," J. Fluid Mech. **177**, 265–292 (1987).

[14] K. Schadow and E. Gutmark, "Combustion instability related to vortex shedding in dump combustors and their passive control," Prog. Energy Combust. Sci. **18**, 117–132 (1992).

[15] C. Coats, "Coherent structures in combustion," Prog. Energy Combust. Sci. **22**, 427–509 (1996).

[16] P.-H. Renard, D. Thevenin, J.-C. Rolon, and S. Candel, "Dynamics of flame/vortex interactions," Prog. Energy Combust. Sci. **26**, 225–282 (2000).

[17] M. P. Juniper and R. Sujith, "Sensitivity and nonlinearity of thermoacoustic oscillations," Annu. Rev. Fluid Mech. **50**, 661–689 (2017).

[18] T. C. Lieuwen, "Experimental investigation of limit-cycle oscillations in an unstable gas turbine combustor," J. Propul. Power **18**, 61–67 (2002).

[19] V. Nair, G. Thampi, S. Karuppusamy, S. Gopalan, and R. Sujith, "Loss of chaos in combustion noise as a precursor of impending combustion instability," Int. J. Spray Combust. Dyn. **5**, 273–290 (2013).

[20] J. Tony, E. Gopalakrishnan, E. Sreelekha, and R. Sujith, "Detecting deterministic nature of pressure measurements from a turbulent combustor," Phys. Rev. E **92**, 062902 (2015).

[21] V. Nair, G. Thampi, and R. Sujith, "Intermittency route to thermoacoustic instability in turbulent combustors," J. Fluid Mech. **756**, 470–487 (2014).

[22] V. Nair and R. Sujith, "Identifying homoclinic orbits in the dynamics of intermittent signals through recurrence quantification," Chaos **23**, 033136 (2013).

[23] V. Nair and R. Sujith, "Multifractality in combustion noise: Predicting an impending combustion instability," J. Fluid Mech. **747**, 635–655 (2014).

[24] H. Gotoda, M. Amano, T. Miyano, T. Ikawa, K. Maki, and S. Tachibana, "Characterization of complexities in combustion instability in a lean premixed gas-turbine model combustor," Chaos **22**, 043128 (2012).

[25] H. Gotoda, Y. Shinoda, M. Kobayashi, Y. Okuno, and S. Tachibana, "Detection and control of combustion instability based on the concept of dynamical system theory," Phys. Rev. E **89**, 022910 (2014).

[26] H. Gotoda, H. Nikimoto, T. Miyano, and S. Tachibana, "Dynamic properties of combustion instability in a lean premixed gas-turbine combustor," Chaos **21**, 013124 (2011).

[27] S. Taamallah, Z. A. LaBry, S. J. Shanbhogue, and A. F. Ghoniem, "Thermo-acoustic instabilities in lean premixed swirl-stabilized combustion and their link to acoustically coupled and decoupled flame macro-structures," Proc. Combust. Inst. **35**, 3273–3282 (2015).

[28] S. Hong, S. J. Shanbhogue, and A. F. Ghoniem, "Impact of fuel composition on the recirculation zone structure and its role in lean premixed flame anchoring," Proc. Combust. Inst. **35**, 1493–1500 (2015).

[29] V. R. Unni and R. Sujith, "Flame dynamics during intermittency in a turbulent combustor," Proc. Combust. Inst. **36**, 3791–3798 (2017).

[30] S. Mondal, V. R. Unni, and R. Sujith, "Onset of thermoacoustic instability in turbulent combustors: An emergence of synchronized periodicity through formation of chimera-like states," J. Fluid Mech. **811**, 659–681 (2017).

[31] A.-L. Barabási, "The network takeover," Nat. Phys. **8**, 14–16 (2012).

[32] D. J. Watts and S. H. Strogatz, "Collective dynamics of'small-world'networks," Nature **393**, 440 (1998).

[33] A.-L. Barabási and R. Albert, "Emergence of scaling in random networks," Science **286**, 509–512 (1999).

[34] B. Albert-László, *Linked: How Everything Is Connected to Everything Else and What It Means for Business, Science, and Everyday Life* (Plume Editors, New York, 2003).

[35] S. Boccaletti, V. Latora, Y. Moreno, M. Chavez, and D.-U. Hwang, "Complex networks: Structure and dynamics," Phys. Rep. **424**, 175–308 (2006).

[36] M. Newman, *Networks: An Introduction* (Oxford University Press, 2010).

[37] A. A. Tsonis and P. J. Roebber, "The architecture of the climate network," Phys. A **333**, 497–504 (2004).

[38] N. Malik, B. Bookhagen, N. Marwan, and J. Kurths, "Analysis of spatial and temporal extreme monsoonal rainfall over south asia using complex networks," Clim. Dyn. **39**, 971–987 (2012).

[39] Z. Gao and N. Jin, "Flow-pattern identification and nonlinear dynamics of gas-liquid two-phase flow in complex networks," Phys. Rev. E **79**, 066303 (2009).

[40] A. Charakopoulos, T. Karakasidis, P. Papanicolaou, and A. Liakopoulos, "The application of complex network time series analysis in turbulent heated jets," Chaos **24**, 024408 (2014).

[41] M. Murugesan and R. Sujith, "Combustion noise is scale-free: Transition from scale-free to order at the onset of thermoacoustic instability," J. Fluid Mech. **772**, 225–245 (2015).

[42] M. Murugesan and R. Sujith, "Detecting the onset of an impending thermoacoustic instability using complex networks," J. Propul. Power **32**, 707–712 (2016).

[43] Y. Okuno, M. Small, and H. Gotoda, "Dynamics of self-excited thermoacoustic instability in a combustion system: Pseudo-periodic and high-dimensional nature," Chaos **25**, 043107 (2015).

[44] V. Godavarthi, V. Unni, E. Gopalakrishnan, and R. Sujith, "Recurrence networks to study dynamical transitions in a turbulent combustor," Chaos **27**, 063113 (2017).

[45] H. Gotoda, H. Kinugawa, R. Tsujimoto, S. Domen, and Y. Okuno, "Characterization of combustion dynamics, detection, and prevention of an unstable combustion state based on a complex-network theory," Phys. Rev. Appl. **7**, 044027 (2017).

[46]J. F. Donges, J. Heitzig, B. Beronov, M. Wiedermann, J. Runge, Q. Y. Feng, L. Tupikina, V. Stolbova, R. V. Donner, N. Marwan *et al.*, "Unified functional network and nonlinear time series analysis for complex systems science: The pyunicorn package," Chaos **25**, 113101 (2015).

[47]R. Q. Quiroga, T. Kreuz, and P. Grassberger, "Event synchronization: A simple and fast method to measure synchronicity and time delay patterns," Phys. Rev. E **66**, 041904 (2002).

[48]N. Boers, B. Bookhagen, H. M. Barbosa, N. Marwan, J. Kurths, and J. Marengo, "Prediction of extreme floods in the eastern central andes based on a complex networks approach," Nat. Commun. **5**, 5199 (2014).

[49]N. Molkenthin, K. Rehfeld, N. Marwan, and J. Kurths, "Networks from flows-from dynamics to topology," Sci. Rep. **4**, 4119 (2014).

[50]L. Tupikina, K. Rehfeld, N. Molkenthin, V. Stolbova, N. Marwan, and J. Kurths, "Characterizing the evolution of climate networks," Nonlinear Processes Geophys. **21**, 705–711 (2014).

[51]K. Taira, P. Munday, and A. Nair, "Understanding the fundamental roles of momentum and vorticity injections in flow control," Tech. Report No. FA9550-13-1-0183 (Florida State University Tallahassee, United States, 2016).

[52]S. Scarsoglio, G. Iacobello, and L. Ridolfi, "Complex networks unveiling spatial patterns in turbulence," Int. J. Bifurcation Chaos Appl. Sci. Eng. **26**, 1650223 (2016).

[53]T. Komarek and W. Polifke, "Impact of swirl fluctuations on the flame response of a perfectly premixed swirl burner," J. Eng. Gas Turbines Power **132**, 061503 (2010).

[54]L. Russo, P. Russo, I. N. Evaggelidis, and C. Siettos, "Complex network statistics to the design of fire breaks for the control of fire spreading," in *Chemical Engineering Transactions* (Italian Association of Chemical Engineering-AIDIC, 2015).

[55]M. Raffel, C. Merz, A. Bauknecht, and T. Schwermer, "High-speed piv, deformation and bos measurements for rotor aero-dynamics," in Proceedings of AFDAR Workshop on Application of Advanced Flow Diagnostics to Aeronautics, Brunswick, Germany (2013).

[56]M. Raffel, C. E. Willert, S. T. Wereley, and J. Kompenhans, "Image evaluation methods for piv," in *Particle Image Velocimetry* (Springer, 2007), pp. 123–176.